

# Optics Letters

## DC-free on-axis holographic display using a phase-only spatial light modulator

JAEBUM CHO,<sup>1</sup> SOOBIN KIM,<sup>2</sup> SHINWOONG PARK,<sup>2</sup> BYOUNGHO LEE,<sup>1</sup> AND HWI KIM<sup>2,\*</sup>

<sup>1</sup>School of Electrical and Computer Engineering, Seoul National University, Gwanak-Gu Gwanakro 1, Seoul 08826, South Korea

<sup>2</sup>Department of Electronics and Information Engineering, Korea University, 2511, Sejong-ro, Sejong 339-700, South Korea

\*Corresponding author: hwikim@korea.ac.kr

Received 7 May 2018; revised 17 June 2018; accepted 19 June 2018; posted 20 June 2018 (Doc. ID 331053); published 12 July 2018

**A DC-noise-free on-axis holographic display scheme using a phase-only spatial light modulator (SLM) is proposed. The origin of DC noise in the on-axis holographic display using a phase-only SLM is analyzed, and a DC noise rejection filter is optimized for a phase-only SLM is designed. A novel two-step iterative Fourier transform algorithm for the optimal synthesis of a phase-only computer-generated hologram using the proposed scheme is devised. The proposed scheme and algorithm are validated with numerical simulations and experiments.** © 2018 Optical Society of America

**OCIS codes:** (050.1970) Diffractive optics; (110.1758) Computational imaging; (090.2870) Holographic display; (090.1995) Digital holography.

<https://doi.org/10.1364/OL.43.003397>

Holographic displays are a promising three-dimensional (3D) display technology [1] with numerous potential applications related to plural 3D display techniques, such as augmented reality displays [2], real volumetric photophoretic trapping displays [3], table-top 3D displays [4], optical security [5], holographic 3D microscopy [6], inspection, and metrology [7]. In a holographic display system, a spatial light modulator (SLM) is commonly used to modulate the incoming light field to a designed holographic field. In practice, the use of SLMs is affected by various forms of noise, such as zero-order and twin-image noise, which arise from the finite pixel size, finite fill factor, and the insufficient dynamic range and precision of the modulation process.

Thus, noise management and filtering techniques are essential to the practical design of holographic display systems. It is well known that zero-order DC noise is generated due to a non-ideal finite fill factor of less than 100% and, particularly, strong DC noise can be harmful to an observer who is directly looking at the holographic display panel. The black matrix section of the SLM is the main cause of zero-order DC noise in a holographic display because the light field imposed on the black matrix becomes a totally controllable specular component. For example, PLUTO (produced by HOLOEYE) has a fill factor of 87% and generates strong DC noise with 13% energy, even when the phase value is modulated exactly as intended.

In Fig. 1, the origin of the DC noise and related issues are presented using a numerical simulation. In Fig. 1(a), a phase-only SLM with a 89% fill factor generates a diffraction image for a computer-generated hologram (CGH) in the image plane. The dark light field blocked by the black matrix pattern of a transmission-type SLM or the bright light field reflected by the black matrix pattern of a reflection-type SLM contributes to an uncontrollable DC noise pattern which is invariant to the dynamic modulation of the SLM pixels, as presented in Fig. 1(b). In Fig. 1(c), the DC pattern and its periodic replication appear at the center of the diffraction image and in the higher-order domain, respectively. In general, to avoid DC noise, the off-axis method is used [8], in which the linear grating phase profile is multiplied by the CGH to shift the signal to the off-axis first order diffraction domain, and a DC-rejection filter masks the zero-order noise formed in the zero-order diffraction domain [9]. This off-axis holographic display setup is widely used for DC noise suppression in holographic displays; in practice, however, it suffers from a technical limitation related to the finite pixel size. In Figs. 1(c) and 1(d), high-order diffraction images with DC noise appearing on the holographic display in on-axis and off-axis modes, respectively, are compared. Because SLM pixels are rectangular, the diffraction image is modulated by a sinc function envelope profile across the higher-order diffraction domain. The problem is that the sinc function contains two-dimensional zero nodal lines, as shown in Figs. 1(c) and 1(d). The lower panels of Figs. 1(c) and 1(d) present the cross-sectional profile of the on-axis and off-axis modes. The on-axis display creates a diffraction image in the main lobe region (the yellow region), while the off-axis mode places the image across the zero node (the red arrow) to keep DC noise from interfering with the diffraction image. The practical obstacle for on-axis holographic displays is the overlap of uncontrollable DC noise and the diffraction image in the zeroth-order domain, while the limitation for the off-axis display mode is the intensity modulation by the sinc envelope profile. Near the zero nodal lines, the sinc profile modulates the diffraction image to be significantly darker; this loss of energy is thought to be an inherent defect of an off-axis holographic display mode which is difficult to eliminate with an SLM that has rectangular pixels.

In this Letter, we propose a DC-noise-free on-axis holographic display and essential algorithm for the optimal synthesis

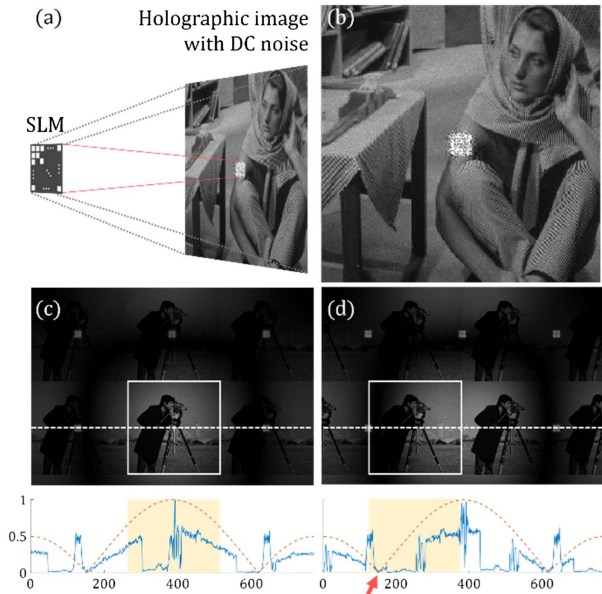


**Fig. 1.** (a) Conventional Fresnel holographic display configuration and (b) the diffraction image with DC noise obtained using the conventional setup. High-order intensity distribution with DC noise of a typical holographic display: (c) on-axis display mode and its cross-sectional profile (blue line) with the sinc envelope (dotted orange line), and (d) off-axis display mode and its cross-sectional profile with the sinc envelope. Note that the peaks in the blue line represent DC noise.

of CGHs for this configuration. In Fourier optics, optical information noise filters typically take the form of an optical Fourier transform-based configuration. For example, the 4-f system-based single-side band holographic display system is convenient [8], but its multiple lenses render it bulky, meaning it cannot be applied in a more compact system configuration. In order to reduce the zero-order DC noise in an on-axis configuration using a single-phase SLM, we need to devise a new type of optical filter and new optimal design algorithm for phase hologram patterns. Figure 2 illustrates a schematic of the proposed system and the CGH synthesis algorithm. A spherically converging wave generated using a convex lens is

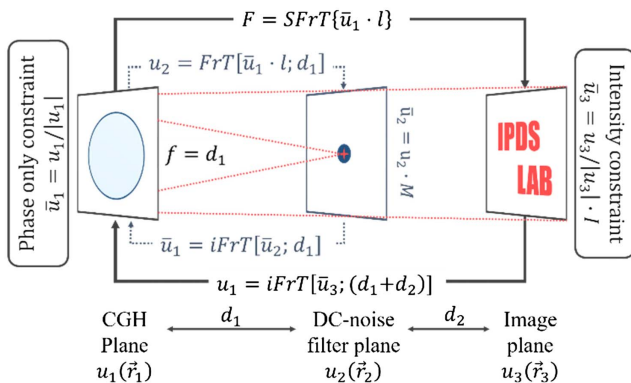


**Fig. 2.** Schematic of the proposed DC-noise-free holographic display system and two-step IFTA for CGH synthesis. The lens behind the SLM represents the spherical backlight carrier wave. Note that the calculation for the small blue loop is already included in the SFrT function, so the large black loop represents the entire calculation process.

incident on the SLM, and the DC component is focused to a point in the focal filtering plane, which can be considered to be a Fourier plane. Although this setup has the advantage that it makes the system more compact compared to the conventional off-axis holographic display configuration, a significant structural issue remains in that the DC-rejection filter may interfere with the signal diffraction field of the CGH, generating a shadow (i.e., a dark field) on the image plane. In order to solve this problem, we modify the CGH to render the shadow of the DC-rejection filter invisible at the image plane and form a designed diffraction image.

In order to realize this scenario, we propose a two-step iterative Fourier transform algorithm (IFTA), illustrated in Fig. 2. This algorithm is an extended version of the conventional IFTA, which takes into account the forward wave propagation from the CGH plane to the image plane passing through the rejection filter plane and the direct backward propagation from the image plane to the CGH plane without interference by the filter. The transforms of the forward and backward propagations are referred to as the sequential Fresnel transform (SFrT) and the inverse Fresnel transform (iFrT), respectively.

The system is composed of two sections: (1) from the CGH plane ( $\vec{r}_1$  plane) to the DC-rejection filter plane ( $\vec{r}_2$  plane), and (2) from the filter plane to the image plane ( $\vec{r}_3$  plane). The distance from the CGH plane to the filter plane and from the filter plane to the image plane are denoted by  $d_1$  and  $d_2$ , respectively. The spherical wave incident on the SLM is represented by  $l(\vec{r}_1)$  and the CGH pattern  $u_1(\vec{r}_1)$  modulates  $l(\vec{r}_1)$  to  $u_1(\vec{r}_1) \cdot l(\vec{r}_1)$  so that the DC noise is focused at the focal point of the incident spherical wave  $l(\vec{r}_1)$ , where the DC noise can be effectively filtered by a rejection filter of minimum diameter (Fig. 2). In most situations,  $d_1$  is set to  $f$ , the focal length of the incident spherical wave  $l(\vec{r}_1)$ . On the filter plane, the center of the light field is blocked by the binary filter mask, denoted by  $m(\vec{r}_2)$ , while the light field passing through the outside of the filter mask continues to propagate to the image plane and form the diffraction image  $u_3(\vec{r}_3)$ . The Fresnel transform,  $\text{FrT}\{f(\vec{r}_1); z\}$ , is defined by

$$\text{FrT}\{f(\vec{r}_1); z\} = \frac{-j}{|\lambda z|} \int_{-\infty}^{+\infty} f(\vec{r}_1) \exp\left\{\frac{j\pi}{\lambda z}(\vec{r}_2 - \vec{r}_1)^2\right\} \vec{r}_1. \quad (1)$$

In this system configuration, the diffraction field,  $u_3(\vec{r}_3)$ , can be calculated using the cascade of the conventional Fresnel transform:

$$u_3(\vec{r}_3) = \text{FrT}\{\text{FrT}\{u_1(\vec{r}_1) \cdot l(\vec{r}_1); d_1\} \cdot m(\vec{r}_2); d_2\}. \quad (2)$$

However, in this case, a numerical problem occurs with respect to the sampling schemes on the image plane. Note that the impulse response form of the Fresnel transform is used instead of the transfer function form. Let the sampling intervals of the CGH plane be  $\Delta\vec{r}_1$ . For Eq. (2), the sampling interval on the image plane  $\Delta\vec{r}_3$  will be  $\Delta\vec{r}_1 d_2 / d_1$ . Let us consider the situation in which the DC-noise filter disappears in space. A single Fresnel transform from the CGH plane to the image plane is described by

$$u_3(\vec{r}_3) = \text{FrT}\{u_1(\vec{r}_1); d_1 + d_2\}. \quad (3)$$

In this case, the sampling interval on the image plane  $\Delta\vec{r}_3$  is  $\lambda(d_1 + d_2) / N\Delta\vec{r}_1$ , where  $N$  is the number of samples. The sampling schemes for Eqs. (2) and (3) contradict each other, since the sampling interval  $\Delta\vec{r}_1$  is proportional to

$\Delta\vec{r}_3$ , according to Eq. (2), while this relationship is reciprocally proportional in Eq. (3). Thus, the discretization processing of the two integral transforms, Eqs. (2) and (3), reveals a mismatch in the sampling scheme. To avoid this problem, the following wave propagation process is adopted. First, optical waves are propagated from the CGH plane to the filter plane; the optical field obscured by the DC-noise mask function  $m(\vec{r}_2)$  is

$$\tilde{u}_2(\vec{r}_2) = m(\vec{r}_2)\text{FrT}\{u_1(\vec{r}_1) \cdot l(\vec{r}_1); d_1\}. \quad (4)$$

Instead of transferring  $\tilde{u}_2(\vec{r}_1)$  to the image plane directly, we use a two-step propagation algorithm. The first step is the iFrT of  $\tilde{u}_2(\vec{r}_1)$  to the CGH plane, and the second step is the forward Fresnel transform of the optical field to the image plane. This two-step propagation is represented by

$$u_3(\vec{r}_3) = \text{FrT}\{\text{iFrT}\{\tilde{u}_2(\vec{r}_2); d_1\}; d_1 + d_2\}. \quad (5)$$

The forward propagation of the entire system can be summarized as the SFrT defined by

$$\begin{aligned} u_3 &= \text{SFrT}\{u_1 \cdot l\} \\ &= \text{FrT}\{\text{iFrT}\{\text{FrT}\{u_1 \cdot l; d_1\} \cdot m; d_1\}; d_1 + d_2\}. \end{aligned} \quad (6)$$

The backward propagation from the image plane to the CGH plane can be written using the iFrT:

$$u_1(\vec{r}_1) = \text{iFrT}\{u_3(\vec{r}_3); d_1 + d_2\}. \quad (7)$$

We can now construct the IFTA using SFrT and iFrT. The resulting flow chart for the proposed IFTA is depicted in Fig. 2. The primary objective of the IFTA is to find a phase-only CGH in the input CGH plane so that the intensity conditions at the image plane are satisfied simultaneously [10,11]. In the proposed IFTA scheme, the filter plane is subject to an additional constraint in that the shadow of the DC-rejection filter should be invisible at the image plane in order to form a designed diffraction image.

In Figs. 3(a) and 3(b), we compare the numerically reconstructed holographic images of CGHs optimized using the two-step

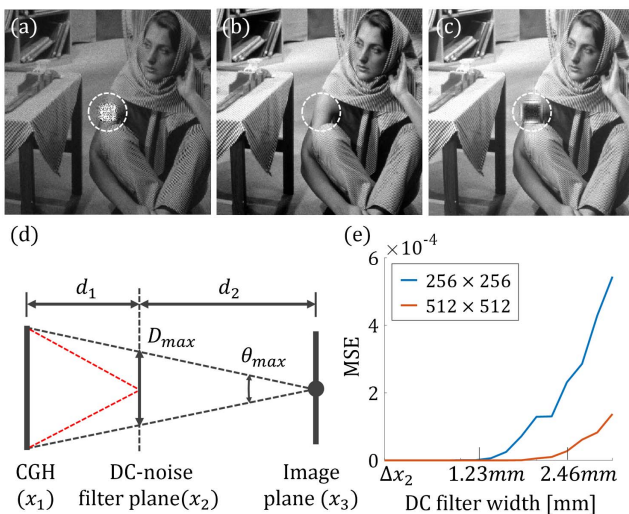


**Fig. 3.** Numerical results of the DC-noise filtering simulation. Diffraction image calculated using the IFTA (a) without a DC-rejection filter and (b) with a 2.4 mm wide DC-rejection filter. (c) Appearance of the shadow of the DC-rejection filter, the size of which (5 mm) is larger than the maximum filter size. (d) Geometrical consideration of the maximum DC-rejection filter size. (e) Relationship between MSE and DC-rejection filter width.

IFTA with and without the DC-rejection filter. The diffraction image without the DC-rejection filter exhibits significant deterioration due to the DC around the center of the image plane [Fig. 3(a)], while the DC noise has been clearly removed from the diffraction with the use of the 2.4 mm  $\times$  2.4 mm rectangular DC-rejection filter [Fig. 3(b)]. There is a limit to the size of the DC-rejection filter, but this can be compensated for in the proposed system.

This means that if the size of the DC-rejection filter goes past its maximum width; a dark shadow cast by the DC-rejection filter begins to appear around the center of the image plane, spreading gradually in the radial direction, with the dark shadow pattern reflecting the diffraction pattern of the shape of the DC-rejection filter [Fig. 3(c)]. For a single point at the center of the image plane of the proposed system, the maximum size of the DC-rejection filter is determined geometrically, as shown in Fig. 3(d). If the DC-rejection filter blocks the entire light path at one point on the image plane, this cannot be resolved, even with the proposed IFTA method. Thus, it is important to design a system so that some part of the light from the CGH plane is delivered to the center region of the output plane without interference by the filter. To achieve this, the maximum diffraction angle,  $\theta_{\max}$ , is given by  $\lambda/\Delta x_3$  at the image plane under paraxial approximation. The maximum width of the DC-blocking filter  $D_{\max}$  can then be determined as

$$D_{\max} = d_2\theta_{\max} = N\Delta x_1 d_2/(d_1 + d_2), \quad (8)$$

where  $N$  is the number of sampling points on one side. Figure 3(e) presents the change in the mean squared error (MSE) for the CGH image by DC-rejection filter width, and the trends support Eq. (8). In the analysis, the pixel pitch of the SLM,  $\Delta x_1$ , is set to 8  $\mu\text{m}$ , and  $d_1$  and  $d_2$  are set to 0.4 and 0.6 m, respectively. When  $N$  is set to 256 and 512, the maximum width of the filter is estimated to be about 1.23 and 2.46 mm, respectively.

In order to validate the proposed system and algorithm, we conducted a holographic display experiment. The proposed system was represented by a simple experimental setup consisting of a He-Ne laser (632 nm), a phase-only SLM (PLUTO of HoloEye Inc.) with a 1920  $\times$  1080 resolution, an 8  $\mu\text{m}$  pixel pitch, and a fill factor of 87%, and conventional 2-in. (50.8 mm) optical components [Fig. 4(a)]. The optical length

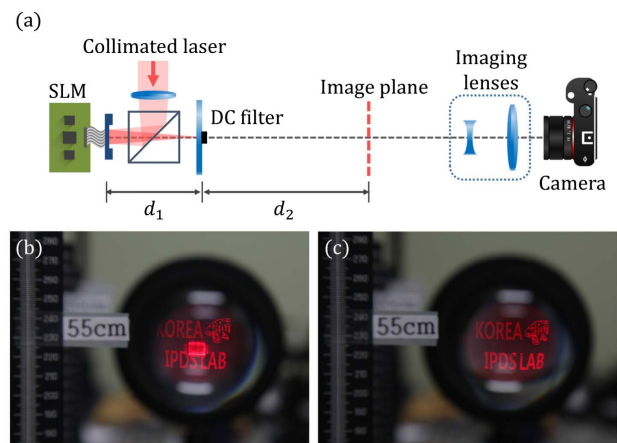


**Fig. 4.** (a) Experimental setup for the holographic 3D display. Experimental results for the filtering DC-noise simulation. (b) Conventional IFTA without a DC-rejection filter. (c) Proposed IFTA with a DC-rejection filter.

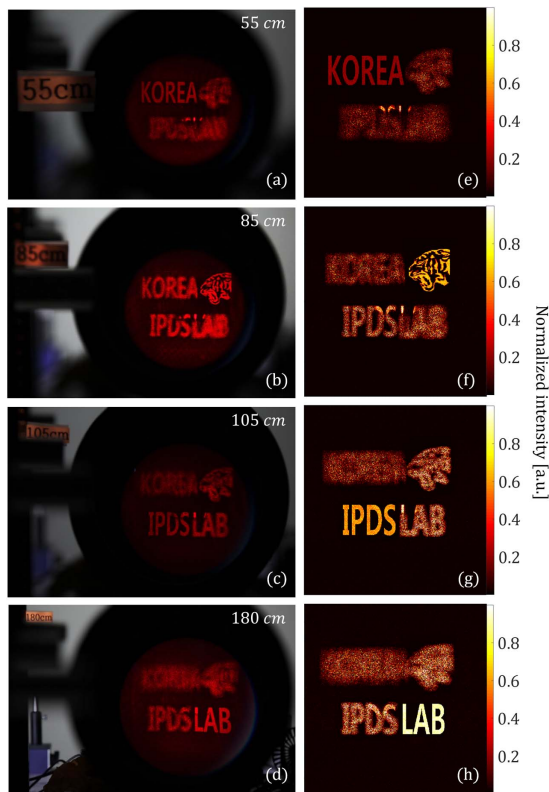


**Fig. 5.** Holographic images of the experimental results with foci at (a) 55, (b) 85, (c) 105, and (d) 180 cm, and the matched numerical results with foci at (e) 55, (f) 85, (g) 105, and (h) 180 cm.

$d_1$  and  $d_2$  are 25 and 55 cm respectively, and the radius of the DC filter is 3 mm. The DC filter is made of round black paper on glass substrate. The first step in the experiment was the optical reconstruction and observation of diffraction images with and without DC noise through a field lens to demonstrate the free holographic 3D display at the single image plane. The experimental results are presented in Figs. 4(b) and 4(c) for clear comparison. The holographic images were taken with a commercial DSLR camera. As previously seen in Fig. 1, a diffraction image affected by DC noise is observed in Fig. 4(b). However, the DC noise can be removed in the same experimental setup by using the DC-rejection filter and the CGH calculated by the proposed method, as shown in Fig. 4(c).

In Fig. 5, we demonstrate the proposed technique for a DC-noise-free on-axis holographic 3D display by presenting for a multi-level depth-map CGH images from both numerical simulations and experiments. For this experiment, we used the two-step IFTA technique to extend the conventional multi-level depth map CGH synthesis algorithm [9]. The application of the

two-step IFTA to multi-level 3D CGH image synthesis is straightforward. The multi-level CGH can be obtained by alternately computing the iterative loops for each depth image. Figures 5(a)–5(d) present observation photos of the holographic 3D images generated by the on-axis holographic display configuration, demonstrating a clear four-depth level accommodation effect. At each depth, the corresponding part of the holographic image comes into focus and the other parts are blurred due to the out-of-focus effect. Although this setup has an on-axis configuration, the DC noise of the phase-only PLUTO SLM was successfully removed and does not affect the resulting holographic 3D image; thus, the DC-rejection filter is invisible to the viewer. These experimental results are further supported by the simulation results in the right column. The left panels of Figs. 5(a) and 5(d) focused on the words “KOREA” and “LAB” separated by 125 cm along the optic axis. Consequently, the proposed holographic display system can successfully express multiple planes focused at different depths with no DC noise.

In conclusion, we have proposed a DC-free on-axis holographic display scheme using a phase-only SLM without DC noise. For this, a two-step IFTA with a DC-rejection filter was devised. The proposed technique can be applied to general holographic 3D display configurations, such as large-aperture and wide-viewing angle multiple SLM array configurations, holographic lithography, holographic trapping, and tweezers, which typically require high energy efficiency.

**Funding.** Korea University (KU).

## REFERENCES

1. J. Hong, Y. Kim, H.-J. Choi, J. Hahn, J.-H. Park, H. Kim, S.-W. Min, N. Chen, and B. Lee, *Appl. Opt.* **50**, H87 (2011).
2. A. Maimone, A. Georgiou, and J. S. Kollin, *ACM Trans. Graph.* **36**, 1 (2017).
3. D. E. Smalley, E. Nygaard, K. Squire, J. Van Wagoner, J. Rasmussen, S. Gneiting, K. Qaderi, J. Goodsell, W. Rogers, M. Lindsey, K. Costner, A. Monk, M. Pearson, B. Haymore, and J. Peatross, *Nature* **553**, 486 (2018).
4. Y. Lim, K. Hong, H. Kim, H.-E. Kim, E.-Y. Chang, S. Lee, T. Kim, J. Nam, H.-G. Choo, J. Kim, and J. Hahn, *Opt. Express* **24**, 24999 (2016).
5. P. Refregier and B. Javidi, *Opt. Lett.* **20**, 767 (1995).
6. D. Gabor, *Nature* **161**, 777 (1948).
7. S. Park, J. H. Lee, and H. Kim, *JSAP-OSA Joint Symposia 2017 Abstracts* (Optical Society of America, 2017), paper 8a\_PB2\_1.
8. H. Kim, C.-Y. Hwang, K.-S. Kim, J. Roh, W. Moon, S. Kim, B.-R. Lee, S. Oh, and J. Hahn, *Appl. Opt.* **53**, G139 (2014).
9. J. Roh, K. Kim, E. Moon, S. Kim, B. Yang, J. Hahn, and H. Kim, *Opt. Express* **25**, 14774 (2017).
10. H. Kim and B. Lee, *Opt. Lett.* **30**, 296 (2005).
11. F. Wyrowski, *J. Opt. Soc. Am. A* **7**, 961 (1990).